Adsorption, Orientation, and Speciation of Amino Acids at Air-Aqueous Interfaces for the Direct Air Capture of CO_2

Nitesh Kumar*, Uvinduni I. Premadasa*, Dengpan Dong, Santanu Roy,
Ying-Zhong Ma, Benjamin Doughty, and Vyacheslav S. Bryantsev*
Chemical Sciences Division, Oak Ridge National Laboratory, Oak Ridge, TN 37831
**E-mail: kumarn@ornl.gov, premadasaui@ornl.gov, bryantsevv@ornl.gov*
(Dated: October 7, 2024)

Amino acids are a promising family of molecules capable of direct air capture (DAC) of CO_2 from the atmosphere. Under alkaline conditions, CO_2 reacts with the anionic form of an amino acid to produce carbamates and deactivated zwitterionic amino acids. The presence of the various species of amino acids and reactive intermediates can have a significant effect on DAC chemistry, the role of which is poorly understood. In this study, all-atom molecular dynamics (MD) based computational simulations and vibrational sum frequency generation (vSFG) spectroscopy studies were conducted to understand the role of competitive interactions at the air-aqueous interface in the context of DAC. We find that the presence of potassium bicarbonate ions, in combination with the anionic and zwitterionic forms of amino acids, induce concentration and charge gradients at the interface, generating a layered molecular arrangement that changes under pre and post-DAC conditions. In parallel, an enhancement in the surface activity of both anionic and zwitterionic forms of amino acids is observed, which is attributed to enhanced interfacial stability and favorable intermolecular interactions between the adsorbed amino acids in their anionic and zwitterionic forms. The collective influence of these competitive interactions, along with the resulting interfacial heterogeneity, may in turn affect subsequent capture reactions and associated rates. These effects underscore the need to consider dynamic changes in interfacial chemical makeup to enhance DAC efficiency and to develop successful negative emission and storage technologies.

Keywords: Direct Air Capture, Negative Emission Technologies, Charged Amino Acids, Interface, Molecular Dynamics Simulations, Vibrational Sum Frequency Generation Spectroscopy.

I. INTRODUCTION

Mitigating climate change and realizing global climate objectives, including limiting the global temperature increase to $< 2°C$, necessitates the deployment of advanced negative emission technologies (NETs) for the selective capture of CO_2 from the atmosphere.[1, 2] Direct air capture (DAC) has garnered significant attention in recent years, primarily because of its potential for deployment at a large scale as a solution to combat climate change.[3, 4] Using liquid absorbents (or solvents), DAC is achieved through chemical reactions that transform CO_2 into carbamates and (bi)carbonates in aqueous media. While aqueous amine-based solvents such as monoethanolamine (MEA) demonstrate efficiency in capturing CO_2,[5, 6] the substantial volumes of air passing over the solvent interface in DAC systems drive solvent evaporation.[7, 8] Therefore, using less volatile compounds like amino acids (AA) in water offers potential benefits in mitigating solvent loss. Consequently, AAs are increasingly recognized as a viable alternative for DAC, as they are nontoxic, biodegradable, easy to synthesize in large quantity, and less susceptible to thermal degradation during CO_2 release and solvent regeneration.[2, 9–12]

In many cases, the aqueous interface serves as a bottleneck for the transfer of CO_2, thereby constraining the rates at which CO_2 can be captured.[13] Therefore, it is crucial to develop a deeper understanding of the chemical and structural changes at the AA-decorated aqueous-air interfaces before and after reactions with CO_2.[14] Recent efforts by our group have provided insight into the interfacial chemistry of AAs utilizing vibrational Sum Frequency Generation (vSFG) spectroscopy and Molecular Dynamics (MD) simulations.[15–17] The evolving bulk phase pH was highlighted as a major driving force that feeds back onto subsequent DAC events and must be contended with in applications. While important, a detailed understanding of AAs on the microscopic level, particularly their average orientation, interactions with other ions, and surface propensities in the presence of DAC products remains poorly understood. Unraveling these interactions and underlying mechanisms is pivotal in the development of efficient interfacial systems for DAC that have the potential to substantially reduce atmospheric CO_2 levels and mitigate the impacts of climate change.

Under alkaline conditions, amino acids (AA) in their anionic form (AA^-) undergo reactions with CO_2, resulting in the formation of dianionic carbamates and corresponding zwitterionic form of the amino acid (AA-zw). Subsequently, the carbamates hydrolyze to form bicarbonate ions (HCO_3^-) and regenerate the anionic form of

the amino acid (AA^-).[8, 18] The appearance of a variety of ionic and charged species during DAC creates competitive conditions for the ions to partition to the interface[19, 20] and subsequently influences the probabilities of CO_2 capture and mechanisms by which DAC can take place.

Herein, we employed MD simulations coupled with the vSFG spectroscopy[21–23] to investigate the interfacial behavior of AA sorbents in the presence of competing ions to provide insight into how competitive ion interactions influence AA adsorption, orientation, and speciation.[24–28] Herein, the interfacial behavior of three AAs (Leu, Val, and Phe) is characterized in the absence and presence of HCO_3^- formed during DAC. We identified a competitive interplay of CO_2 reaction products at the interface that must be balanced to maintain the surface activity of reactive AA^- in facilitating interfacial CO_2 transport and sustaining high capture rates.

II. RESULTS AND DISCUSSION

In this study, two distinct DAC-related systems were simulated. The first is an air-aqueous system containing AAs at high pH (pH 12, AA^-), which is compared to a similar system at a neutral pH (pH 7, AA-zw). Charge balance was maintained by adding potassium (K^+) ions. The second system contained a mixture of AA^- and AA-zw in the presence of HCO_3^-, mimicking the CO_2 loaded solutions after DAC. This composition should be considered an idealized mixture because, under DAC conditions, the equilibrated reaction mixtures include other DAC products such as CO_3^{2-} and carbamates. However, the majority of the carbonaceous ions present in the medium would be HCO_3^-.[8, 15]

A. Interfacial Properties of Amino Acids at High and Neutral pH

We started by characterizing the adsorption behaviors of AAs at the air-aqueous interface at both neutral and elevated pHs, with the latter representing the initial conditions used in DAC reactions. To quantify this adsorption behavior, we generated normalized density profiles to the center of mass of the carbon atoms of the isopropyl side groups of Val and Leu, and the center of mass of the carbon atoms of the phenyl ring in Phe (Figure 1 C-E). Of the three, the hydrophobic side chain of Leu exhibited the highest interfacial propensity. This observation aligns with the prominent CH vibrations detected for Leu in vSFG measurements, indicating AA^- species within the interfacial region. Although the enhanced adsorption of AA could improve DAC efficiency, this is not the sole factor influencing CO_2 chemical conversion at the interface. Factors such as the specific orientation and desolvation of -NH_2 and CO_2 are crucial for effective interactions and chemical conversion. Thus, DAC efficiency is determined by an interplay of adsorption, orientation, and specific coordination environment. Furthermore, the zwitterionic forms of AA exhibit higher adsorption propensity at the interface compared to their anionic counterparts across all three AAs. This observation is consistent with both our current and previous work, which showed stronger spectral signatures in vSFG upon reducing the pH, both in the presence and absence of CO_2.[15]

TABLE I: Average interfacial tilt and twist angle of AAs in their pure anionic and zwitterionic forms. The interfacial region is determined based on one or two standard deviations (σ or 2σ) derived from fitting the interfacial density profiles to a Gaussian distribution function. The measured tilt and twist angles exhibit minimal sensitivity to the specified width of the interface. The values were rounded off to three significant figures.

System	Tilt angle° (σ, 2σ)	Twist angle° (σ, 2σ)
Val^-	37.5, 37.9	55.4, 55.9
Val-zw	53.9, 54.4	52.3, 51.9
Leu^-	43.5, 43.5	41.3, 41.3
Leu-zw	36.1, 35.4	38.9, 36.4
Phe^-	65.8, 62.0	44.1, 44.3
Phe-zw	54.1, 53.6	44.4, 44.5

Since vSFG spectroscopy is sensitive to variations in both surface concentration and orientation, it is essential to establish an understanding of how AAs are positioned at the interface. The orientation of the alkyl and aryl groups at the interface can be defined using three Euler angles, θ, ψ, and ϕ, as visualized in Figure 1 B. Following previous conventions[29–31] the tilt angle θ is defined as the angle between the bisector of the plane formed by the carbon atoms of the isopropyl or phenyl group, $\hat{v}$ and the surface normal, $\hat{z}$. The twist angle ψ is the angle between the plane defined by the carbon atoms of the isopropyl or phenyl group and the plane formed by the symmetry axis $\hat{v}$ and the surface normal. The azimuthal angle of $\hat{v}$ around the $\hat{z}$ axis in the x-y plane is isotropically distributed between 0 and 2π and is therefore averaged over.

The variations in the average tilt angles as a function of a distance from the interface for different AAs in their anionic and zwitterionic forms are plotted in Figure 1 F-H. An average value of 90° in the bulk aqueous phase ($\langle cos\theta \rangle = 0$) is observed for all systems, indicating random orientations where the likelihood of observing angles between 0 and 180° is equally probable.[19] As AAs approach the interface, they continue to exhibit a wide ori-

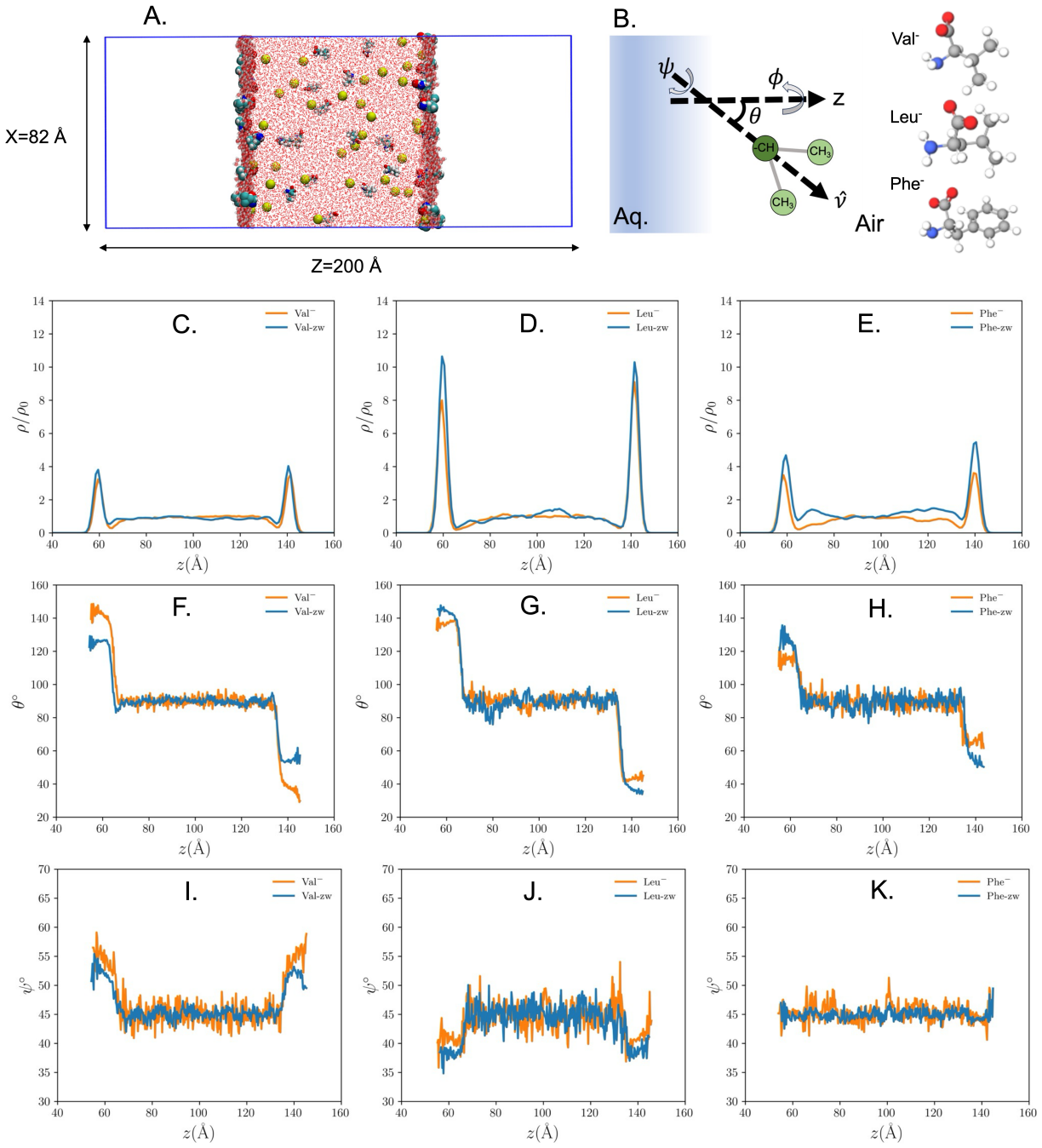

FIG. 1: An illustration of the air-aqueous system investigated in the present study. The molecules in the instantaneous layers directly in contact with the air phase are highlighted by an increased size of the atoms. The carbon, oxygen, nitrogen, hydrogen, and potassium atoms are colored in cyan, red, blue, white, and yellow, respectively. (B) The schematic illustration of the tilt (θ) and twist angles (ψ) of the terminal isopropyl group, as defined in the text. The structures of Val^-, Leu^- and Phe^- are provided in the inset. Normalized density profiles (ρ/ρ_0, where ρ_0 is the bulk density) along z-axis of the center of mass of the terminal isopropyl group of (C) Val (D) Leu in the anionic (AA^-) and zwitterionic forms (AA-zw), and (E) the benzyl group of Phe in the anionic and zwitterionic states and the corresponding tilt (F-H) and twist angles (I-K). An average θ value of 90° in the bulk phase denotes a random orientation of molecules within the bulk aqueous phase. Similarly, an average ψ value of 45° in the bulk phase signifies that molecules show an equal probability of having a clockwise or anticlockwise twist.

entational distribution, as indicated in Figure S1. Nevertheless, they tend to align at the interface with their

hydrophobic tails preferentially directed towards the air phase and their polar groups facing the aqueous phase, as shown in Figure 1 A. For Val, the anionic form is tilted more than the zwitterionic form, whereas the reverse trend is observed for Leu and Phe. This behavior is associated with the presence of an extra -CH_2- group connecting the alkyl and phenyl groups to the remaining parts of Leu and Phe, respectively, increasing the complexity of the conformational landscape as a result of larger conformational flexibility of Leu compared to Val. This is confirmed by employing the CREST-xtb approach,[32] as illustrated in Figure S2, and is primarily characterized by variations in the internal carbon bond dynamics and their rotational freedom, in contrast to the simpler conformational profile observed for Val.

To determine the average orientational angles at the interface, it is necessary to define the boundaries of the interfacial region. We accomplished this by fitting AA density profiles to a Gaussian function, as depicted in Figure S3. For each AA, we selected the interfacial region as the area extending one standard deviation σ from the mean in the Gaussian distribution function and then computed the average orientation within this region. Extending the width of the interfacial region from σ to 2σ leads to only minor changes in the average angles, indicating that the results are relatively insensitive to the specific choice of interfacial length. Data presented in Table I reveal distinct orientational trends for anionic and zwitterionic forms of AAs. In particular, within the group of anionic AAs, Val exhibits a more structured orientation, whereas Phe predominantly displays a less organized orientation relative to the bulk. Among the zwitterionic AA, Leu-zw stands out as having the most pronounced ordered orientation, while Phe consistently exhibits the least ordered orientation. We extended our analysis by computing the cumulative orientation profiles using the formula:

$$\langle \rho' \rangle \langle \cos\theta \rangle$$

where, ρ' is the normalized density profile, $\cos\theta$ is the cosine of the tilt angle, and the angle brackets represent averages over each window (Figure S4). The magnitude of the cumulative orientation profile qualitatively corresponds to the peak intensities measured in the vSFG spectra.[33, 34]

The magnitude of the cumulative orientation profile qualitatively corresponds to the peak intensities measured in the vSFG spectra. The experimental vSFG data plotted in Figure 2 consistently corroborates our MD findings. While the changes in line shapes from experimental data are indicative of changing populations, orientation, and interference of SFG signals from overlapping resonances, MD findings inform the origin of these peak changes. Leu displays notably larger cumulative peaks in Figure S4 compared to both Val and Phe. This is primarily attributed to the greater surface affinity of Leu relative to the other amino acids. Similarly, zwitterionic Leu and Phe exhibit notably higher intensities compared to their anionic counterparts. This increase in intensity can be attributed to the combined influence of both improved adsorption and stronger orientational alignment for the zwitterionic forms of Leu and Phe compared to their anionic forms. Nonetheless, when it comes to Val, our observations deviate from the vSFG results showing higher peak intensities for the zwitterionic form. We, instead, observed similar peak intensities in the cumulative orientation profiles. This is due to two opposing factors influencing the cumulative profile, i.e., the Val-zw form has stronger adsorption while its tilt angle is smaller. This discrepancy underscores the importance of taking into account the contributions arising from twist angles as well. Following the twist angle definition given above, a ψ value of 0° signifies that the plane defined by the carbon atom of the isopropyl or phenyl group is orthogonal to the xy plane, while a value of 90° indicates that the two carbon atoms on the opposite sides of the C2 axis are symmetrically positioned relative to the xy plane. In the bulk aqueous phase, this angle can take a random value from 0 to 90°, averaging to ψ=45°($\cos 2\psi$ =0). The variations in the twist angles as a function of z for three studied AA are shown in Figure 1 (I-K), while the corresponding distributions at the interface can be found in Figure S5. Our findings indicate that Phe, irrespective of its ionic state, does not show a preference for any particular twist angle at the interface. As a result, the influence of the twist angle on the vSFG intensity can be reliably disregarded. In contrast, both Val and Leu exhibit substantial deviations from the bulk averaged twist angle as they approach the interface. Val^- shows the largest twist angle (55-56°), which has the strongest effect on decreasing the vSFG intensity (i.e., $\cos 2\psi < 0$).[35] The inclusion of the twist angle, in conjunction with the cumulative orientational profile, is essential for a more thorough interpretation of the experimental vSFG spectra of Val.

To shed light on the orientation preferences of hydrophilic groups in AAs, we analyzed the tilt angles of the vectors formed between the α-carbon (C_α) and the N (NH_2/NH_3^+) or the C (COO^-) atoms relative to the surface normal for both AA^- and AA-zw (refer to Figure S6). It is observed that charged COO^- and NH_3^+ groups predominantly tilts towards the aqueous phase, while the orientation of the NH_2 group is more subtle, exhibiting only weak orientation preference compared to the bulk. The charged COO^- group is more strongly oriented toward the aqueous phase and is positioned deeper inside

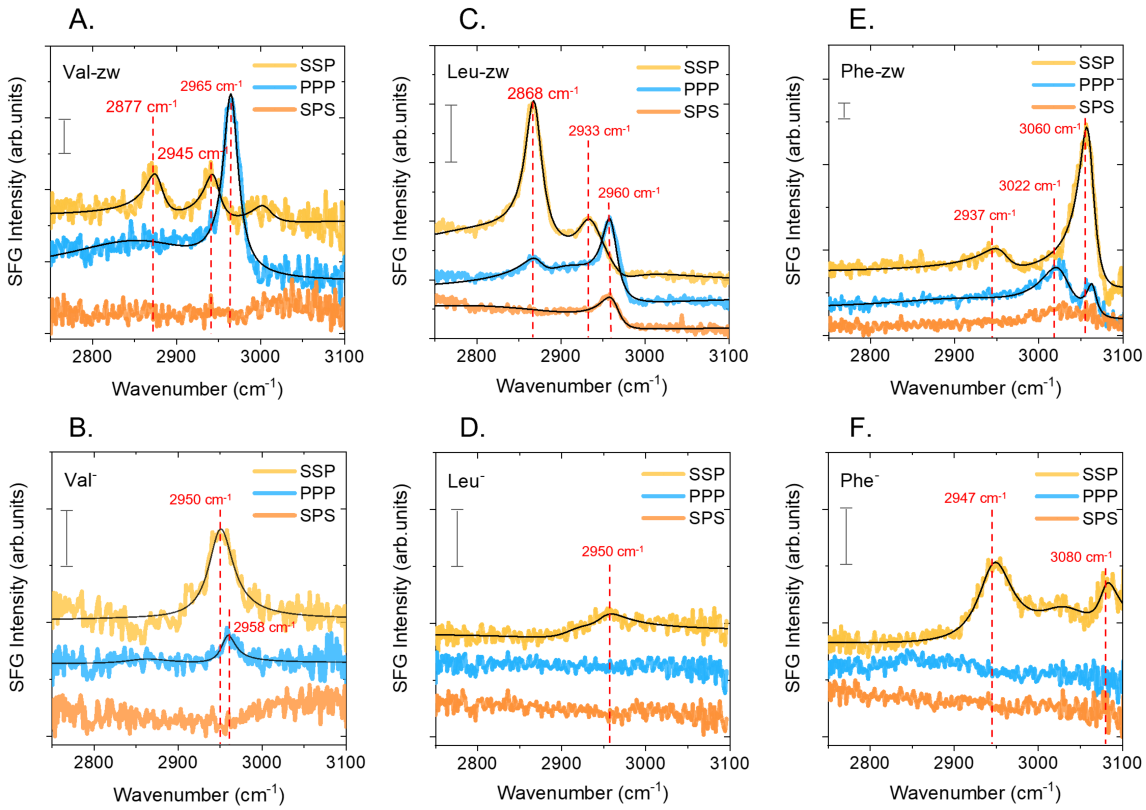

FIG. 2: VSFG spectra from Val (A, B), Leu (C, D), and Phe (E, F) in their neutral or zwitterionic form at pH $\sim$ 7 (top row) and anionic forms at pH $\sim$ 12 (bottom row) collected at three different polarization combinations. The scale bar in each plot corresponds to $\sim$ 0.5 arb. units. Black lines are the fits to experimental data using Eq.1. Spectra are vertically offset for clarity.

this phase compared to the NH_3^+ group. This is consistent with the previous study[15, 36] suggesting that the COO^- group tends to retain a full hydration shell near the interface, while the NH_3^+ group is afforded to loose up to one water molecule. The orientation of these AA at the interface, especially the reactive -NH_2 group and associated solvation shells, might be important to CO_2 capture/conversion chemistries without affecting the overall capacity. The weaker solvation of the reactive -NH_2 group at the interface could potentially lead to faster reaction kinetics with CO_2 owing to the rate-limiting step being the nucleophilic attack by the -NH_2 group on the electropositive carbon atom of CO_2.[16, 37]

We acquired vSFG spectra from different polarization combinations to probe the average orientations at the interface (Figure 2). Fit peak amplitudes and widths of the methyl ($-CH_3$) asymmetric stretch (AS) at 2960 cm^{-1} at SPS and PPP polarization combination were used for extracting orientational information for Leu. We employed the method reported by Cremer et.al[30] where the hyperpolarizabilities of the two individual methyl groups in the molecular frame were combined to derive the nonlinear susceptibility of the isopropyl group ($-C(CH_3)_2$) in the laboratory frame.[38] As this results in a set of twist-tilt angle combinations (orange curve in Figure S7), we consider the orientation of the -CH group to narrow down the range of solutions for tilt-twist angles of the methyl bisector.[35, 38] Agreeing with simulation results, minimal/zero signal observed from the -CH group vibrations suggests that this group is oriented parallel to the surface plane (Figure S8). Note that the angle between this -CH and $-C(CH_3)_2$ groups should be $\sim 120°$ based on the effective trigonal planar arrangement of unique functional groups. From this, the dot product between the two vectors pointing along the bond axes constrains the solutions that are possible, as was done for the similar isopropyl groups.[35, 38] We find the set of orientational values that the $-CH_3$ group bisectors can take when -CH is tilted $\sim 90°$ from the surface normal (Figure S9). For Leu in its zwitterionic form, we find that $-C(CH_3)_2$ bisector is tilted at angle $\sim 36 \pm 1°$ with a twist angle of $\sim 58 \pm 1°$. We note here that the small error bars stem from uncertainties in fitting and should be considered a lower limit to the true experimental uncertainty. The

agreement between experiment and simulation for the tilt angles is quite good but differs somewhat in the twist angles, which implies the existence of missing interactions in simulations and/or underscores limiting assumptions made in vSFG analysis. Our testing of three different force fields indicates that their influence on the twist angle of Leu^- is rather small, giving a consistent value close to 40° (Figure S10). We emphasize that the twist angle distribution at the interface spans the entire spectrum of possible values (Figure S5), leading to a relatively small free energy difference among different orientations that are averaged over in experiment. Future studies may explore the potential for improving agreement with experimental results by explicitly accounting for polarizability effects in the force field and experimental efforts directed to quantify orientational distributions with vSFG.[39, 40]

While we do not observe the required vibrational modes to quantify orientational angles from anionic Leu or from Val, we can provide qualitative insight to compare with simulations. For zwitterionic Val, given that $-CH_3AS$ mode in PPP polarization has significantly higher intensity compared to $-CH_3$ SS in SSP polarization, it is apparent that the $-CH_3$ groups are tilted closer to the surface than towards the surface normal.[41] This result agrees with what was obtained from simulations. To assess the orientation of the phenyl group, we consider the ratio between aromatic -CH symmetric mode (v_2) at 3060 cm^{-1} observed in SSP and PPP polarization combinations (Figure S9). Here, the hyperpolarizability ratio ($r = \frac{\beta_{aac}}{\beta_{ccc}}$) was taken to be in the range 0.8-0.9.[42] Using these parameters, and neglecting quadrupole contributions, we find that the phenyl ring is tilted at an angle $60 \pm 6°$ when the twist angles are averaged as revealed by simulations.[43] Overall, the experimental and simulation results show close correspondence and therefore successfully benchmark the results reported in this study.

Building on this agreement between experiment and simulation, we turn attention to the presence of DAC species at the interface and how they can exert unexpected and nontrivial effects on the propensity of other ions to approach the interface.[44, 45]

Consequently, we observe that the presence of anionic AAs at the interface causes K^+ ions to partition into the electric double layer. As can be seen from Figure 4, the changes in the normalized density profiles of K^+ follow the same trend as those of AA^- counterions, confirming the electrostatic nature of these interactions. This co-localization results in both contact and solvent-separated ion pairing[46] as illustrated in Figure 3 by the increased first and second peaks of $g(r)$ compared to those in the bulk. Given the work by Cremer and coworkers showing that the mode of ion pairing does not necessarily follow

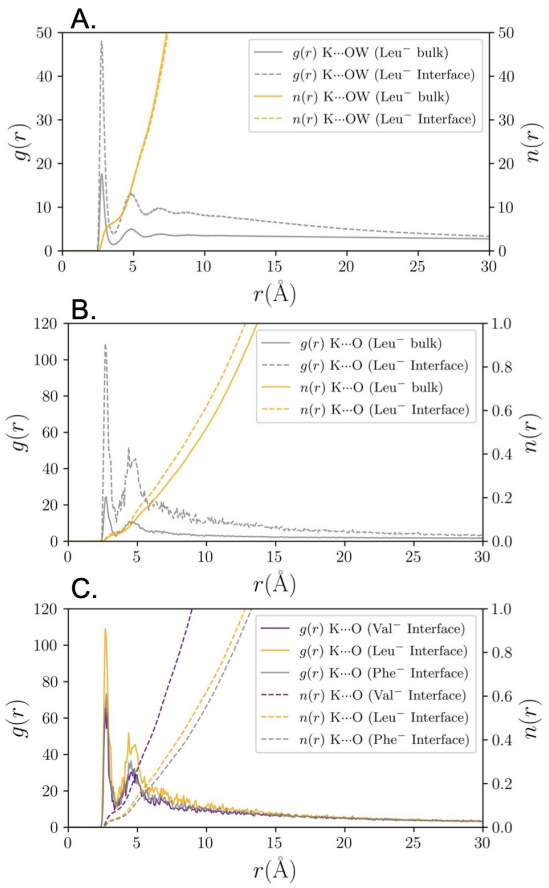

FIG. 3: (A) Radial distribution functions, $g(r)$, and coordination numbers, $n(r)$, between the K^+ ions and water oxygen atoms (O_W) in the bulk and at the air-aqueous interface for the Leu system. (B) $g(r)$ and $n(r)$ between the K^+ ions and oxygen atoms of AA (COO^-) in the bulk and at the air-aqueous interface for the Leu system. (C) $g(r)$ and $n(r)$ between the K^+ ions and oxygen atoms of three AA (COO^-) at the air-aqueous interface.

equilibrium binding affinities,[46] we do not attempt to differentiate between pairing mechanisms in this work. Separate experiments and simulations investigating these details in DAC systems are underway.

Similar results have been discussed in the partitioning of carbonate to interfaces as accompanied by Na^+ ions.[47] Such behavior is driven by ion-ion interactions at the interface, which can be elucidated by examining radial distribution functions ($g(r)$) within the interfacial region.[48] We defined this area by selecting a 20 Å slab, beginning at the z-coordinate where the water density decreases to zero (immediately before it transitions to the air phase), and extending 20 Å into the water phase. As depicted in Figure 3 A, there is a pronounced enhancement in the interactions of K^+ ions with water at the interface compared to bulk. A similar trend was ob-

served for K^+ interactions with oxygen atoms (O) of the carboxylate groups (COO^-) of AA^-, as shown in Figure 3 B.

This highlights a significant increase in the interaction between K^+ and Leu^- at the interface compared to the bulk phase. The interfacial interactions between K^+ ions and Leu^- are notably stronger than those with Val^- and Phe^- ions, as illustrated in Figure 3 C. The preceding analysis suggests that the zwitterionic form of AA exhibits a higher degree of surface activity compared to the anionic form of AA. This implies that as AA^- converts into AA-zw during DAC, the latter is likely to accumulate at the interface, potentially reducing the efficiency of DAC.

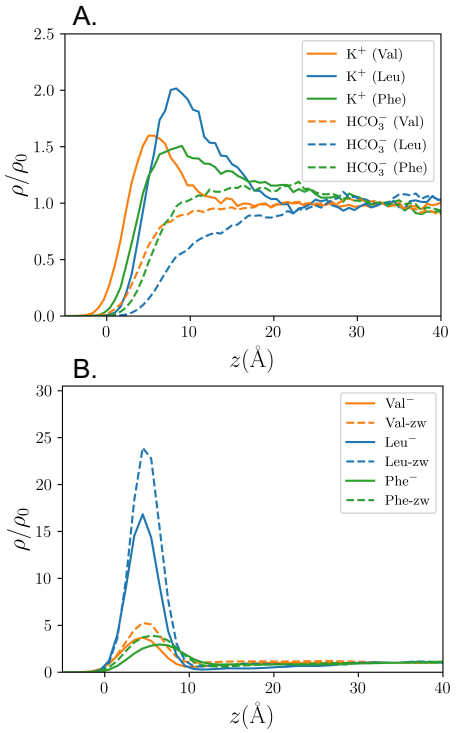

FIG. 4: Normalized density profiles as a function of the distance z from the air-aqueous interface in the 1:1:1 mixture of HCO_3^-, AA^-, and AA-zw for (A) K^+ and HCO_3^- ions, (B) the isopropyl group of Val and Leu and the phenyl group of Phe in their anionic and zwitterionic forms. The z=0 represents the location of the Gibbs dividing surface, where the density of water is quantified to be 0.5× of its value in bulk.

B. Interfacial Properties of Mixtures Containing Reactants and Products of DAC

In our efforts to gain a more comprehensive understanding of how DAC products influence their preference for the aqueous-air interface and the accompanying interactions, we adopted a model consisting of a 1:1:1 mixture of HCO_3^-, AA^-, and AA-zw. This composition approximates the distribution at equilibrium following DAC. We did not include dianionic carbamate species in simulations given that for the concentration range of AAs studied here, hydrolysis leads to the formation of HCO_3^- as the primary capture product. In future investigations, we plan to explore AAs with greater solubility and explicitly account for the presence of dianionic carbamates that might partition to the surface in the presence of coordinating counterions.[49] This will require a comparison of the performance of nonpolarizable and polarizable force fields, which is beyond the scope of the current work.

Our results indicate that K^+ ions exhibit a stronger affinity ($\sim 2\times$) for the interface region (below Gibbs dividing surface) compared to bulk in the presence of interfacial AAs. In contrast, bicarbonate ions are significantly less prevalent in this region, acting as typical hard anion that tends to avoid the interface, partitioning well below the Gibbs dividing surface (Figure 4 A). This is further characterized using the radial distribution functions as shown in Figure S11 where both anionic and zwitterionic forms exhibited strong interactions with K^+ ions at the interface, whereas bicarbonate primarily demonstrated strong interaction only with the K^+ ion. To investigate the impact of the concentration gradient created by ions on the adsorption properties of AAs, we analyzed the normalized density profiles, tilt and twist orientations along z axis, and the cumulative orientation profiles (Figure 4 B and Figure S12-14) for the anionic and zwitterionic forms of these AAs in the mixture system. As shown in Figure 4 B, we noted a slight increase in the normalized density for Val and Phe within the mixture, whereas there was a marked enhancement in the normalized density of both the anionic and zwitterionic forms of Leu (more than 2×) when compared to their isolated states. The intermolecular $g(r)$ depicted in Figure S15-17, clearly show that the adsorption of AA at the interface results in a substantial increase in intermolecular interactions between their anionic and zwitterionic forms, greatly surpassing those in the bulk aqueous phase. This increase in the interaction strength is consistent across all three AAs, with Leu displaying the most pronounced effect (Figure S16). Consequently, the enhanced stability of Leu in the mixture at the interface is associated with an increase in intermolecular ion interactions between anionic and zwitterionic forms in the interfacial region.

In contrast to the variations in concentration profiles of the mixtures, the molecular orientation at the interface is only slightly affected. The average values of the tilt and twist angles of AAs in the mixtures are provided in Table S2. The AA in the mixture displayed similar

orientation trends as observed in the pure systems. The concentration gradient at the air-water interface leads to a slightly more structured orientation of AAs in the mixture compared to the anion-only system. This is indicated by a reduction in the average tilt angle, with the observed deviation staying within about 5 degrees compared to the angles in the pure systems. Thus, even with increased adsorption, the orientation of the AAs at the interface is primarily controlled by the strong hydration of the charged and polar groups and the unfavorable interactions of the hydrophobic groups with water.

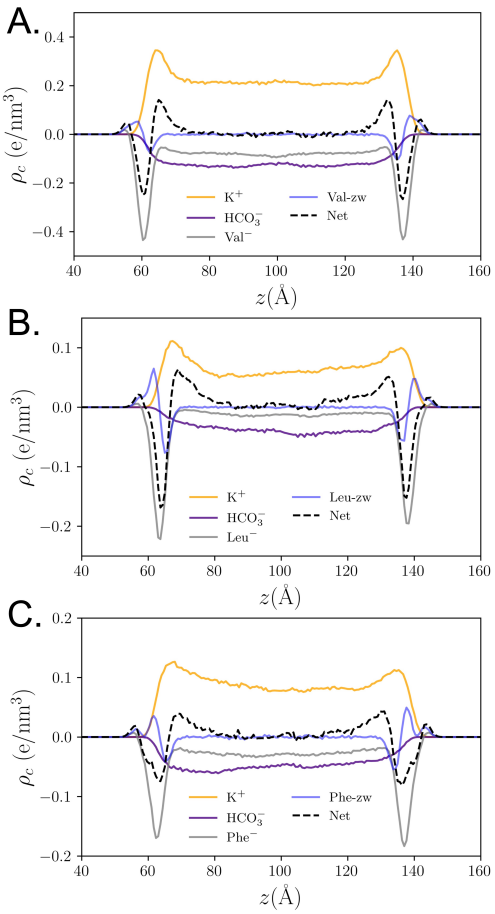

FIG. 5: Charge density (ρ_c) profiles of ions (K^+ and HCO_3^-), the AAs in their anionic and zwitterionic forms (AA^- and AA-zw), and the net charge density profiles along the z axis for (A) Val (B) Leu and (C) Phe in the 1:1:1 mixture of HCO_3^-, AA^-, and AA-zw.

For a more comprehensive understanding of the molecular distribution at the interface, we analyzed the charge density profiles[45] of K^+, HCO_3^-, AA^-, and AA-zw for the three AA systems, as depicted in Figure 5. These profiles detail the specific contributions of individual molecules to the charge gradient present at the interface[50, 51]. The combined charge density of all ions displays a double layer type charge distribution, as indicated by the dashed black lines. We observe a pronounced anionic excess in the region adjacent to the air phase, attributed predominantly to the anionic AA^- form of the AA. The zwitterionic AA exhibits a distinct spatially varying charge density distribution pattern at the interface. This is characterized by a double-layer type of charge density, wherein the NH_3^+ group is located closer to the interface, while the COO^- group is positioned further away from the interface in the aqueous phase, as also evidenced from the differences in their tilt angles (Figure S6). The predominant contributors to the cationic excess in the adjacent layer are the K^+ ions. It is clear from these profiles that HCO_3^- remained subsurface and has a secondary role in the double layer-like charge density distribution at the interface.[52]

III. CONCLUSIONS

In summary, our study integrated MD simulations and surface-sensitive vSFG spectroscopy to explore the effects of competitive ion interactions on the behavior of amino acids at the interface, a vital aspect to the DAC of CO_2. We analyzed AA adsorption and average molecular orientation at the interface, before and after DAC, using normalized density profiles and computing tilt and twist angles. Our results showed favorable adsorption of the three AAs, with the zwitterionic forms showing a higher propensity for the interface compared to the anionic forms. The hydrophobic side chains were oriented towards the air phase and the charged NH_3^+ and COO^- groups were directed towards the aqueous phase. Subsequently, our computational results were verified using experimental data obtained from vSFG spectroscopic measurements. We observed that the orientation of the reactive NH_2 group at the interface is influenced by the nature of AA, showing weak preferences for orientation towards either the air or the bulk. Modulating the -NH_2 orientation by controlling the solvation via surfactant-decorated interfaces could be one way to improve the kinetics of DAC. Our results also underscore that the mixture of the DAC reaction products, namely HCO_3^-, AA-zw, and AA^-, induce both concentration and charge gradients in the interfacial region. In this scenario, HCO_3^- ions are primarily located in the subsurface region, while K^+ ions show a tendency to gather at the interface in the presence of DAC reaction products. Our results of modeling a fixed composition containing AA^- reactants and AA-zw products of DAC suggest an increase in intermolecular interactions between AA-zw and AA^- at the interface, resulting in better co-adsorption of both the

anionic and zwitterionic forms of AA. We postulate that the accumulation of these DAC reaction products intensifies molecular crowding at the interface, which could contribute to enhanced interfacial viscosity and potentially diminish the overall efficacy of DAC over time. To mitigate this effect, we are exploring several strategies to modulate surface makeup using surfactants with charged groups to regulate ion-ion interactions and photoresponsive materials to control interfacial pH.

IV. MATERIALS AND METHODS

Molecular Dynamics Simulations

All-atom molecular dynamics simulations were performed using the GROMACS software package.[53] In this study, we adopted a simulation protocol similar to the methodology presented in ref. 15. The system compositions are provided in the SI. To simulate the specific pH environment, we utilized AA species that are dominant at a given pH. A short-range cutoff of 15Å is utilized for the non-bonded interactions. The long-range electrostatic interactions were modeled using the Particle-Mesh Ewald (PME) methodology.[54] Periodic boundary conditions were employed in all three directions. Each system was simulated for a minimum of 150 ns, where the initial 100 ns were used as equilibration, and the last 50 ns were used for data analysis. Molecular motions were performed using a 1 fs timestep at 300 K and using the leap-frog verlet algorithm. Water is represented using the TIP4P/2005 model[55] and the AAs were modeled using the OPLS-AA force fields. Accurate modeling of the interfacial behavior of AA requires robust benchmarking, comparison of different combinations of force fields, and comparison with experimental properties.[56–58] We tested three different force fields, OPLS-AA,[59, 60] AMBER and CHARMM,[61] as described in the Supplementary Information. Each force field reproduced the experimentally observed interfacial tension (γ) displayed in Figure S18 and, in line with experimental findings, showed an enhanced density within the interfacial region (Figure S19) and higher cumulative intensity of zwitterionic over anionic forms of Phe at the air-water interface, as illustrated in Figure S20. Following our previous work, the OPLS-AA force field was used in the final production runs.[15]

Experimental Details

Materials. All chemicals were purchased from Sigma-Aldrich except for leucine which was purchased from Alfa Aesar. These chemicals were used without further purification, with their respective purities as follows: l-valine (98%), l-leucine (99%), l-phenylalanine (98%), and KOH (99.99%). For vSFG measurements, samples were dissolved in ultrapure water (18.2 MΩ cm). Anionic AA solutions were prepared and the final pH of the solutions was adjusted to 12.0 by adding drops of concentrated KOH. The concentrations of AA solutions prepared were 380, 115, and 150 mM for valine, leucine, and phenylalanine, respectively, and were close to their solubility limits. Effective DAC of CO_2 requires the use of concentrated AA solutions. Therefore, AA concentrations close to the solubility limit were selected for this study to investigate surface structuring in DAC applications. Measurements were made immediately after sample preparation to limit (slow) CO_2 capture and interactions of carbonaceous salts. We also note that in preparing pH 7 samples we did not add any KOH to the medium. All three AAs have pK_{a2} in the range of 9.1–9.6. At pH 7, zwitterions are the major species whereas at pH 12, anions are the dominant species.

Vibrational Sum Frequency Generation (vSFG) Spectroscopy. All experiments were performed using a home-built vSFG spectrometer; details of this instrument can be found in our previous publication.[62] vSFG spectra were collected with 15 minutes camera exposures in SSP, PPP, and SPS polarization combinations (S and P refers to the polarizations of the vSFG, NIR, and IR fields, respectively). The spectra were background-subtracted, normalized to a reference spectrum taken from a gold film, and fit to:

$$I_{\mathrm{SFG}} \propto \left| \chi^{(2)}_{\mathrm{NR}} e^{i\phi} + \sum_q \frac{A_q}{\omega_{\mathrm{IR}} - \omega_q + i\gamma_q} \right|^2 \qquad (1)$$

where ω_q, A_q, and Γ_q are resonant frequencies, amplitudes, and line widths for the various modes. ω_{IR} is the IR frequency, χ_{NR} is the nonresonant contribution, and ϕ is the phase angle.[63, 64] Fitting results are provided in Table S6-9. VSFG spectra peak assignments are provided in Table S10.

Acknowledgments

This research was supported by the US Department of Energy, Office of Science, Basic Energy Sciences, Chemical Sciences, Geosciences, and Biosciences Division, Separation Sciences. This work was produced by UT-Battelle LLC under Contract No. AC05-00OR22725 with the U. S. Department of Energy. This research used resources of the Oak Ridge Leadership Computing Facility at the Oak Ridge National Laboratory, which is sup-

ported by the Office of Science of the U.S. Department of Energy under Contract No. DE-AC05-00OR22725.

Supplementary Information

Additional computational results including density profiles; tilt and twist angles, cumulative orientation profiles; radial distribution functions; interfacial tensions; and comparison of normalized density and cumulitive profiles using three different force fields.

Public Access Statement

Author Contribution

NK, DD, SR, and VB contributed to the computational study. UP, YM, and BD contributed to the vSFG study. The manuscript was written through the contributions of all authors. All authors have given approval to the final version of the manuscript.

[1] Hanna, R.; Abdulla, A.; Xu, Y.; Victor, D. G. Emergency deployment of direct air capture as a response to the climate crisis. *Nature Communications* **2021**, *12*, 368.

[2] Brethomé, F. M.; Williams, N. J.; Seipp, C. A.; Kidder, M. K.; Custelcean, R. Direct air capture of CO2 via aqueous-phase absorption and crystalline-phase release using concentrated solar power. *Nature Energy* **2018**, *3*, 553–559.

[3] Sanz-Pérez, E. S.; Murdock, C. R.; Didas, S. A.; Jones, C. W. Direct capture of CO2 from ambient air. *Chemical Reviews* **2016**, *116*, 11840–11876.

[4] Erans, M.; Sanz-Pérez, E. S.; Hanak, D. P.; Clulow, Z.; Reiner, D. M.; Mutch, G. A. Direct air capture: process technology, techno-economic and socio-political challenges. *Energy & Environmental Science* **2022**, *15*, 1360–1405.

[5] Sinopoli, A.; Abotaleb, A.; Pietrucci, F.; Gladich, I. Stability of a Monoethanolamine-CO2 Zwitterion at the Vapor/Liquid Water Interface: Implications for Low Partial Pressure Carbon Capture Technologies. *The Journal of Physical Chemistry B* **2021**, *125*, 4890–4897.

[6] Lepaumier, H.; Picq, D.; Carrette, P.-L. New amines for CO2 capture. I. Mechanisms of amine degradation in the presence of CO2. *Industrial & Engineering Chemistry Research* **2009**, *48*, 9061–9067.

[7] Filburn, T.; Helble, J.; Weiss, R. Development of supported ethanolamines and modified ethanolamines for CO2 capture. *Industrial & Engineering Chemistry research* **2005**, *44*, 1542–1546.

[8] Custelcean, R. Direct Air Capture of CO2 Using Solvents. *Annual Review of Chemical and Biomolecular Engineering* **2022**, *13*, 217–234.

[9] Ramezani, R.; Mazinani, S.; Di Felice, R. State-of-the-art of CO2 capture with amino acid salt solutions. *Reviews in Chemical Engineering* **2022**, *38*, 273–299.

[10] Sang Sefidi, V.; Luis, P. Advanced amino acid-based technologies for CO2 capture: A review. *Industrial & Engineering Chemistry Research* **2019**, *58*, 20181–20194.

[11] Sumida, K.; Rogow, D. L.; Mason, J. A.; McDonald, T. M.; Bloch, E. D.; Herm, Z. R.; Bae, T.-H.; Long, J. R. Carbon dioxide capture in metal–organic frameworks. *Chemical Reviews* **2012**, *112*, 724–781.

[12] Lyu, H.; Li, H.; Hanikel, N.; Wang, K.; Yaghi, O. M. Covalent organic frameworks for carbon dioxide capture from air. *Journal of the American Chemical Society* **2022**, *144*, 12989–12995.

[13] Ruiz-Lopez, M. F.; Francisco, J. S.; Martins-Costa, M. T.; Anglada, J. M. Molecular reactions at aqueous interfaces. *Nature Reviews Chemistry* **2020**, *4*, 459–475.

[14] Ozkan, M.; Nayak, S. P.; Ruiz, A. D.; Jiang, W. Current status and pillars of direct air capture technologies. *iScience* **2022**, *25*, 103990.

[15] Premadasa, U. I.; Dong, D.; Stamberga, D.; Custelcean, R.; Roy, S.; Ma, Y.-Z.; Bocharova, V.; Bryantsev, V. S.; Doughty, B. Chemical Feedback in the Self-Assembly and Function of Air–Liquid Interfaces: Insight into the Bottlenecks of CO2 Direct Air Capture. *ACS Applied Materials & Interfaces* **2023**, *15*, 19634–19645.

[16] Premadasa, U. I.; Kumar, N.; Zhu, Z.; Stamberga, D.; Li, T.; Roy, S.; Carrillo, J.-M. Y.; Einkauf, J. D.; Custelcean, R.; Ma, Y.-Z.; Bocharova, V.; Bryantsev, V. S.; Doughty, B. Synergistic Assembly of Charged Oligomers and Amino Acids at the Air–Water Interface: An Avenue toward Surface-Directed CO2 Capture. *ACS Applied Materials & Interfaces* **2024**, *16*, 12052–12061.

[17] Angle, K. J.; Nowak, C. M.; Davasam, A.; Dommer, A. C.; Wauer, N. A.; Amaro, R. E.; Grassian, V. H.

Amino acids are driven to the interface by salts and acidic environments. *The Journal of Physical Chemistry Letters* **2022**, *13*, 2824–2829.

[18] Yoon, B.; Voth, G. A. Elucidating the Molecular Mechanism of CO2 Capture by Amino Acid Ionic Liquids. *Journal of the American Chemical Society* **2023**, *145*, 15663–15667.

[19] Kumar, N.; Servis, M. J.; Liu, Z.; Clark, A. E. Competitive interactions at electrolyte/octanol interfaces: A molecular perspective. *The Journal of Physical Chemistry C* **2020**, *124*, 10924–10934.

[20] Luo, G.; Malkova, S.; Yoon, J.; Schultz, D. G.; Lin, B.; Meron, M.; Benjamin, I.; Vanysek, P.; Schlossman, M. L. Ion distributions near a liquid-liquid interface. *Science* **2006**, *311*, 216–218.

[21] Nihonyanagi, S.; Yamaguchi, S.; Tahara, T. Ultrafast dynamics at water interfaces studied by vibrational sum frequency generation spectroscopy. *Chemical Reviews* **2017**, *117*, 10665–10693.

[22] Morita, A.; Hynes, J. T. A theoretical analysis of the sum frequency generation spectrum of the water surface. *Chemical Physics* **2000**, *258*, 371–390.

[23] Liu, D.; Ma, G.; Levering, L. M.; Allen, H. C. Vibrational spectroscopy of aqueous sodium halide solutions and air- liquid interfaces: Observation of increased interfacial depth. *The Journal of Physical Chemistry B* **2004**, *108*, 2252–2260.

[24] Sun, P.; Binter, E. A.; Vo, T.; Benjamin, I.; Bera, M. K.; Lin, B.; Bu, W.; Schlossman, M. L. Relevance of Surface Adsorption and Aqueous Complexation for the Separation of Co (II), Ni (II), and Fe (III). *The Journal of Physical Chemistry B* **2023**, *127*, 3505–3515.

[25] Kumar, N.; Clark, A. E. Adsorbate Organization Characterized by Sublevelset Persistent Homology. *Journal of Chemical Theory and Computation* **2023**, *19*, 3303–3312.

[26] Vácha, R.; Slavícek, P.; Mucha, M.; Finlayson-Pitts, B. J.; Jungwirth, P. Adsorption of atmospherically relevant gases at the air/water interface: Free energy profiles of aqueous solvation of N2, O2, O3, OH, H2O, HO2, and H2O2. *The Journal of Physical Chemistry A* **2004**, *108*, 11573–11579.

[27] Kikkawa, S.; Amamoto, K.; Fujiki, Y.; Hirayama, J.; Kato, G.; Miura, H.; Shishido, T.; Yamazoe, S. Direct air capture of CO2 using a liquid amine–solid carbamic acid phase-separation system using diamines bearing an aminocyclohexyl group. *ACS Environmental Au* **2022**, *2*, 354–362.

[28] Benjamin, I. Chemical reactions and solvation at liquid interfaces: A microscopic perspective. *Chemical Reviews* **1996**, *96*, 1449–1476.

[29] Ji, N.; Shen, Y.-R. Sum frequency vibrational spectroscopy of leucine molecules adsorbed at air–water interface. *The Journal of Chemical Physics* **2004**, *120*, 7107–7112.

[30] Kataoka, S.; Cremer, P. S. Probing molecular structure at interfaces for comparison with bulk solution behavior: Water/2-propanol mixtures monitored by vibrational sum frequency spectroscopy. *Journal of the American Chemical Society* **2006**, *128*, 5516–5522.

[31] Lu, X.; Spanninga, S. A.; Kristalyn, C. B.; Chen, Z. Surface orientation of phenyl groups in poly (sodium 4-styrenesulfonate) and in poly (sodium 4-styrenesulfonate): poly (3, 4-ethylenedioxythiophene) mixture examined by sum frequency generation vibrational spectroscopy. *Langmuir* **2010**, *26*, 14231–14235.

[32] Pracht, P.; Bohle, F.; Grimme, S. Automated exploration of the low-energy chemical space with fast quantum chemical methods. *Physical Chemistry Chemical Physics* **2020**, *22*, 7169–7192.

[33] Ishiyama, T.; Terada, D.; Morita, A. Hydrogen-bonding structure at zwitterionic lipid/water interface. *The journal of Physical Chemistry letters* **2016**, *7*, 216–220.

[34] Karnes, J. J.; Gobrogge, E. A.; Walker, R. A.; Benjamin, I. Unusual Structure and Dynamics at Silica/Methanol and Silica/Ethanol Interfaces A Molecular Dynamics and Nonlinear Optical Study. *The Journal of Physical Chemistry B* **2016**, *120*, 1569–1578.

[35] Doughty, B.; Goverapet Srinivasan, S.; Bryantsev, V. S.; Lee, D.; Lee, H. N.; Ma, Y.-Z.; Lutterman, D. A. Absolute molecular orientation of isopropanol at Ceria (100) surfaces: Insight into catalytic selectivity from the interfacial structure. *The Journal of Physical Chemistry C* **2017**, *121*, 14137–14146.

[36] Herboth, R.; Gopakumar, G.; Caleman, C.; Wohlert, M. Charge State Dependence of Amino Acid Propensity at Water Surface: Mechanisms Elucidated by Molecular Dynamics Simulations. *The Journal of Physical Chemistry A* **2021**, *125*, 4705–4714.

[37] Ma, X.; Bryantsev, V. S.; Roy, S. An ab initio free energy study of the reaction mechanism and rate-limiting steps of CO2 capture by aqueous glycine. *Cell Reports Physical Science* **2023**, *4*.

[38] Tan, S.; Gray, M. B.; Kidder, M. K.; Cheng, Y.; Daemen, L. L.; Lee, D.; Lee, H. N.; Ma, Y.-Z.; Doughty, B.; Lutterman, D. A. Insight into the selectivity of isopropanol conversion at strontium titanate (100) surfaces: A combination kinetic and spectroscopic study. *ACS Catalysis* **2017**, *7*, 8118–8129.

[39] Rao, Y.; Hong, S.-Y.; Turro, N. J.; Eisenthal, K. B. Molecular orientational distribution at interfaces using second harmonic generation. *The Journal of Physical Chemistry C* **2011**, *115*, 11678–11683.

[40] Kundu, A.; Watanabe, H.; Yamaguchi, S.; Tahara, T. Agreement between experimentally and theoretically estimated orientational distributions of solutes at the air/water interface. *The Journal of Physical Chemistry C* **2013**, *117*, 8887–8891.

[41] Wang, H.-F.; Velarde, L.; Gan, W.; Fu, L. Quantitative sum-frequency generation vibrational spectroscopy of molecular surfaces and interfaces: lineshape, polarization, and orientation. *Annual Review of Physical Chemistry* **2015**, *66*, 189–216.

[42] Bzeih, W.; Gheribi, A.; Wood-Adams, P. M.; Hayes, P. L. Dependence of the surface structure of polystyrene on chain molecular weight investigated by sum frequency generation spectroscopy. *The Journal of Physical Chem-*

istry C **2018**, *122*, 3838–3845.

[43] Matsumura, F.; Yu, C.-C.; Yu, X.; Chiang, K.-Y.; Seki, T.; Bonn, M.; Nagata, Y. Does the Sum-Frequency Generation Signal of Aromatic C–H Vibrations Reflect Molecular Orientation? *The Journal of Physical Chemistry B* **2023**, *127*, 5288–5294.

[44] Seki, T.; Yu, C.-C.; Chiang, K.-Y.; Greco, A.; Yu, X.; Matsumura, F.; Bonn, M.; Nagata, Y. Ions Speciation at the Water–Air Interface. *Journal of the American Chemical Society* **2023**, *145*, 10622–10630.

[45] Kumar, N.; Servis, M. J.; Clark, A. E. Uranyl speciation in the presence of specific ion gradients at the electrolyte/organic interface. *Solvent Extraction and Ion Exchange* **2022**, *40*, 165–187.

[46] Judd, K. D.; Gonzalez, N. M.; Yang, T.; Cremer, P. S. Contact Ion Pair Formation Is Not Necessarily Stronger than Solvent Shared Ion Pairing. *The Journal of Physical Chemistry Letters* **2022**, *13*, 923–930.

[47] Jubb, A. M.; Hua, W.; Allen, H. C. Organization of water and atmospherically relevant ions and solutes: vibrational sum frequency spectroscopy at the vapor/liquid and liquid/solid interfaces. *Accounts of Chemical Research* **2012**, *45*, 110–119.

[48] Kumar, N.; Clark, A. E. Unexpected inverse correlations and cooperativity in ion-pair phase transfer. *Chemical Science* **2021**, *12*, 13930–13939.

[49] Devlin, S. W.; Jamnuch, S.; Xu, Q.; Chen, A. A.; Qian, J.; Pascal, T. A.; Saykally, R. J. Agglomeration Drives the Reversed Fractionation of Aqueous Carbonate and Bicarbonate at the Air–Water Interface. *Journal of the American Chemical Society* **2023**, *145*, 22384–22393.

[50] Ober, P.; Boon, W. Q.; Dijkstra, M.; Backus, E. H.; van Roij, R.; Bonn, M. Liquid flow reversibly creates a macroscopic surface charge gradient. *Nature Communications* **2021**, *12*, 4102.

[51] Poli, E.; Jong, K. H.; Hassanali, A. Charge transfer as a ubiquitous mechanism in determining the negative charge at hydrophobic interfaces. *Nature Communications* **2020**, *11*, 901.

[52] Litman, Y.; Chiang, K.-Y.; Seki, T.; Nagata, Y.; Bonn, M. Surface stratification determines the interfacial water structure of simple electrolyte solutions. *Nature Chemistry* **2024**, 1–7.

[53] Van Der Spoel, D.; Lindahl, E.; Hess, B.; Groenhof, G.; Mark, A. E.; Berendsen, H. J. GROMACS: fast, flexible, and free. *Journal of Computational Chemistry* **2005**, *26*, 1701–1718.

[54] Darden, T.; York, D.; Pedersen, L. Particle mesh Ewald: An N log (N) method for Ewald sums in large systems. *The Journal of Chemical Physics* **1993**, *98*, 10089–10092.

[55] Abascal, J. L.; Vega, C. A general purpose model for the condensed phases of water: TIP4P/2005. *The Journal of Chemical Physics* **2005**, *123*.

[56] Dasetty, S.; Meza-Morales, P. J.; Getman, R. B.; Sarupria, S. Simulations of interfacial processes: recent advances in force field development. *Current Opinion in Chemical Engineering* **2019**, *23*, 138–145, Frontiers of Chemical Engineering: Molecular Modeling.

[57] Kumar, N.; Sadhu, B.; Clark, A. E. Essential Aspects of Solvent Effects and Solution Conditions upon the Modeling and Simulation of Lanthanide and Actinide Complexes. *Rare Earth Elements and Actinides: Progress in Computational Science Applications* **2021**, 249–276.

[58] Kumar, N. Exclusive ion recognition using host–guest sandwich complexes. *Phys. Chem. Chem. Phys.* **2024**, *26*, 3152–3158.

[59] Jorgensen, W. L.; Tirado-Rives, J. Potential energy functions for atomic-level simulations of water and organic and biomolecular systems. *Proceedings of the National Academy of Sciences* **2005**, *102*, 6665–6670.

[60] Kaminski, G. A.; Friesner, R. A.; Tirado-Rives, J.; Jorgensen, W. L. Evaluation and reparametrization of the OPLS-AA force field for proteins via comparison with accurate quantum chemical calculations on peptides. *The Journal of Physical Chemistry B* **2001**, *105*, 6474–6487.

[61] Vanommeslaeghe, K.; Hatcher, E.; Acharya, C.; Kundu, S.; Zhong, S.; Shim, J.; Darian, E.; Guvench, O.; Lopes, P.; Vorobyov, I.; others CHARMM general force field: A force field for drug-like molecules compatible with the CHARMM all-atom additive biological force fields. *Journal of Computational Chemistry* **2010**, *31*, 671–690.

[62] Chowdhury, A. U.; Watson, B. R.; Ma, Y.-Z.; Sacci, R. L.; Lutterman, D. A.; Calhoun, T. R.; Doughty, B. A new approach to vibrational sum frequency generation spectroscopy using near infrared pulse shaping. *Review of Scientific Instruments* **2019**, *90*, 033106.

[63] Premadasa, U. I.; Bocharova, V.; Lin, L.; Genix, A.-C.; Heller, W. T.; Sacci, R. L.; Ma, Y.-Z.; Thiele, N. A.; Doughty, B. Tracking Molecular Transport Across Oil/Aqueous Interfaces: Insight into "Antagonistic" Binding in Solvent Extraction. *The Journal of Physical Chemistry B* **2023**, *127*, 4886–4895.

[64] Ohno, P. E.; Wang, H.-f.; Geiger, F. M. Second-order spectral lineshapes from charged interfaces. *Nature communications* **2017**, *8*, 1032.